Progress In Electromagnetics Research, Vol. 142, 639–665, 2013

POLARIMETRIC SAR MODEL FOR SOIL MOISTURE ESTIMATION OVER VINEYARDS AT C-BAND

J. David Ballester-Berman*, Fernando Vicente-Guijalba, and Juan M. Lopez-Sanchez

Signals, Systems and Telecommunication Group, University of Alicante, Alicante 03080, Spain

Abstract—In this paper we propose a two-component polarimetric model for soil moisture estimation on vineyards suited for C-band radar data. According to a polarimetric analysis carried out here, this scenario is made up of one dominant direct return from the soil and a multiple scattering component accounting for disturbing and non-modeled signal fluctuations from soil and short vegetation. We propose a combined X-Bragg/Fresnel approach to characterize the polarized direct response from soil. A validation of this polarimetric model has been performed in terms of its consistency with respect to the available data both from RADARSAT-2 and from indoor measurements. High inversion rates are reported for different phenological stages of vines, and the model gives a consistent interpretation of the data as long as the volume component power remains about or below 50% of the surface contribution power. However, the scarcity of soil moisture measurements in this study prevents the validation of the algorithm in terms of the accuracy of soil moisture retrieval and an extensive campaign is required to fully demonstrate the validity of the model. Different sources of mismatches between the model and the data have been also discussed and analyzed.

1. INTRODUCTION

Soil moisture is a key factor driving the hydrological processes that take place on Earth's surface. Some of these processes are linked to the development of agricultural crops where the efficient management of water resources is a critical factor. Hence, the remote sensing community is focused on the design of tools capable of detecting the

Received 17 July 2013, Accepted 16 September 2013, Scheduled 9 October 2013

* Corresponding author: Josep David Ballester-Berman (davidb@ua.es).

water stress of crops within wide areas and defining the irrigation needs of plants. Those tools are even much more efficient when they provide both high spatial and temporal resolutions. In this context, satellite radar sensors constitute unique systems for such a purpose.

The main problem for soil moisture estimation in a vegetated area, based on radar data as input, is the effect of the vegetation layer on the radar returns. While in case of bare surfaces there are several techniques that deal successfully with the problem by means of either semi-empirical models [1–4] or polarimetric approaches [5], the situation becomes more complicated in vegetated terrain [6–8]. A multi-angular approach at C-band was proposed in [9] by using empirical relationships based on backscattering coefficients. In [10] crop-independent empirical relationships are designed to infer vegetation height, soil roughness and water content from a multi-polarization acquisition of RADARSAT-2 data with accuracies of 19%, 10% and 25.5%, respectively. From these estimates the soil moisture is subsequently retrieved with a 32% relative error. A further improvement over methods using only the intensity values consists in including the relative phase information of the polarimetric measurements and, hence, correlations between channels. In this line, the application of model-based decomposition schemes has shown great potential in order to increase the performance of retrieval algorithms at L-band [11–13]. However, at higher frequencies further research is still required although some progress has been already made [14].

In [15] an in-deep analysis on the polarimetric response from vineyards at C-band data acquired by RADARSAT-2 was performed. Time series of backscattering coefficients, eigendecomposition parameters and complex correlation of copolar channels were computed, and it was shown that the electromagnetic response from this scene is made up of a strong direct return from soil and a weak and variable depolarized return due to the development of plants (i.e., grape bunches and leaf area index — LAI — variations). This previous analysis suggests that vineyards can be modeled as a two-component scenario composed by a Bragg (or X-Bragg) surface and a depolarizing target which accounts for both vegetation variation throughout the phenological cycle and propagation effects due to roughness variations within the field. This concept is exploited in this work to extend to C-band the applicability of radar polarimetry (PolSAR) to soil moisture inversion.

The paper is organized as follows. Section 2 is devoted to recall some of the fundamental advances of polarimetric SAR modeling that have been considered in the design of the model we propose. In Section 3 a two-component polarimetric model suited for vineyards will be proposed and justified. Besides the ideas recalled from [15]

for the justification of such a model, some additional evidences aimed at demonstrating the suitability of the two-component model to the scene under study are in order, hence, Section 3 will be also dedicated to this purpose. In particular we will show how the typical Bragg (or X-Bragg) model for surface electromagnetic characterization of rough soils covers only partially the scattering events generated by such a scene. Therefore, in line with the work in [14], we propose to interpret direct ground response as a combined X-Bragg/Fresnel model. To this aim, polarimetric data set acquired at the European Microwave Signature Laboratory (EMSL) at JRC-Ispra (Italy) over a rough surface will be also analyzed for justifying this interpretation. In Section 4, the soil moisture inversion algorithm will be presented, and several issues related to the inversion procedure will be likewise discussed. Retrieval results will be presented and analyzed in Section 5. Finally, the main conclusions of this work will be summarized in Section 6.

2. FUNDAMENTALS ON MODEL-BASED POLSAR MODELING

The Freeman-Durden decomposition [16, 17] is one of the most important techniques for PolSAR data exploitation due to both its relative simplicity and its capability for interpreting the scattering mechanisms associated with different physical elements in natural and man-made environments. This technique assumes that the covariance/coherency matrix of the backscattering data can be decomposed into three covariance/coherency matrices corresponding to direct surface (odd-bounce), dihedral-type (double or even-bounce) and a random volume. The 3×3 coherency matrix $\mathbf{T}$ can be modeled with the well-known expression given in Eq. (1) [18]:

$$\mathbf{T} = f_s \begin{bmatrix} 1 & \beta^* & 0 \\ \beta & |\beta|^2 & 0 \\ 0 & 0 & 0 \end{bmatrix} + f_d \begin{bmatrix} |\alpha|^2 & \alpha & 0 \\ \alpha^* & 1 & 0 \\ 0 & 0 & 0 \end{bmatrix} + \frac{f_v}{4} \begin{bmatrix} 2 & 0 & 0 \\ 0 & 1 & 0 \\ 0 & 0 & 1 \end{bmatrix} \quad (1)$$

where the first term in the right side relates to the direct surface contribution, the second one to the dihedral scattering, and the third one to the contribution of a randomly oriented set of dipoles.

In recent years some improvements of the Freeman-Durden model have been proposed to deal with limitations and inconsistencies of such a model. In [19] a helix component was also included in the method and a simple threshold-based rule for deciding the type of volume was proposed. Actually, the modeling of volume component is regarded as the main source of inaccuracy of the original approach since the

random cloud of dipoles does not always fit the physics underlying the different natural media. Some attempts have been investigated and proposed in order to cope with this problem. In [20, 21] the authors investigated the issue of negative power of the remainder after subtraction of the volume component and introduced a new approach consisting in modulating the contribution attributed to the volume by means of a nonnegative eigenvalue constraint. Alternatively, in [22] the assumption of a forest volume as a maximum entropy scenario was implemented jointly with deorientation [23–25] of the coherency matrix for minimizing the cross-polar channel. Another different strategy has been aimed at the improvement of the flexibility of the volume model. In [26] a generalized volume component was developed which includes two adjustment factors, i.e., a particle shape parameter [27] and the copolarized ratio. In [28] a generalized orientation angle probability density function was introduced and it was used in order to devise an adaptive decomposition scheme in [29]. More recently, an empirical model where PolInSAR coherences are used to fit the volume scattering in a adaptive way on a pixel-by-pixel basis has been proposed [30]. This empirical model allows an increased dynamic range of the volume power which leads to avoid the overestimation of the volume component. Further improvements have been proposed in [31] where authors have demonstrated that volume scattering power can be uniquely determined as the minimum generalized eigenvalue of the eigenproblem defined by Eq. (2):

$$\mathbf{T} \cdot \mathbf{x} = \lambda \cdot \mathbf{T_{vol}} \cdot \mathbf{x} \tag{2}$$

where $\mathbf{T}$ is the measured coherency matrix, $\mathbf{T_{vol}}$ the volume coherency matrix, and λ the generalized eigenvalue corresponding to the associated eigenvector $\mathbf{x}$.

Also, Lee et al. [32] have proposed an integral approach based on the original Freeman-Durden decomposition. Authors have thoroughly analyzed the deficiencies of existing approaches and they have proposed some modifications in order to overcome them (specially the negative power issue) while retaining the original characteristics of the original approach by Freeman and Durden. Notwithstanding all these improvements, so far there is no clear evidence that allows us to make an a priori selection of one of these volume models among all the rest for polarimetric SAR data exploitation. Contrarily, it seems that for a given practical problem the more appropriate strategy would be to select the volume scattering model in accordance to a previous analysis on the SAR data and/or an a priori knowledge of the properties of the natural cover. This would be indeed a reasonable strategy for PolSAR modeling when the target can be modeled as a dominant rank-

1 component and a weak depolarized return which acts as a sort of source of disturbing effects on the desired strong polarized component. This is the key idea of the Huynen decomposition which has been somehow taken into consideration on later works such as the two-component decomposition by Freeman for mixed natural media [27], the surface depolarization model proposed by Allain [33], and also the two-component model adopted for rice scenes at X-band with dual-polarized data [34]. Actually, this rank-1 plus depolarizing component model theoretically describes the behavior we found in vineyards in our polarimetric study performed in [15] at C-band. In this scenario the direct ground scattering dominates consistently the response along the phenological cycle and, on the other hand, the combined effect of high roughness conditions at C-band and presence of vine plants induces multiple scattering events which incoherently add to the polarized ground return. This idea was also discussed in [35] where the effect of the order of the multiple scattering term on a polarized structure was studied.

3. PROPOSED MODEL

According to the previous lines, we propose to model the vineyards scenario has a two-component model made up of one dominant direct return from the soil and a multiple scattering component accounting for disturbing and non-modeled signal fluctuations from soil and short vegetation. The general model is given in Eq. (3):

$$\mathbf{T} = f_s \begin{bmatrix} 1 & \beta^* \cdot \mathrm{sinc}2\psi & 0 \\ \beta \cdot \mathrm{sinc}2\psi & \frac{1}{2}|\beta|^2 \cdot (1 + \mathrm{sinc}4\psi) & 0 \\ 0 & 0 & \frac{1}{2}|\beta|^2 \cdot (1 - \mathrm{sinc}4\psi) \end{bmatrix} + f_{ms} \begin{bmatrix} t_{11}^{ms} & t_{12}^{ms} & 0 \\ t_{12}^{ms^*} & t_{22}^{ms} & 0 \\ 0 & 0 & t_{33}^{ms} \end{bmatrix} \tag{3}$$

The first term in the summation represents the soil surface characterized by the X-Bragg model proposed in [5], which accounts for depolarization and cross-polarized signal from the ground. The validity range of such a model covers the scenarios where the vertical roughness (represented by s) fulfils the condition $k \cdot s < 1$, where $k = 2\pi/\lambda$. At C-band (e.g., 5.4 GHz for RADARSAT-2) this leads to approximately $s = 1$ cm, which is expected to fall outside the soil roughness conditions in the test sites of this study according to the ground-truth reports (see also Fig. 2). However, in this work we postulate that the addition of a second non-dominant term accounting for multiple scattering events

produced at both ground and volume layers can be used to correctly retrieve some properties of the scene.

The structure of the multiple scattering component is represented by the second term in the summation of Eq. (3). Previous works in the literature have pointed out that the multiple scattering contribution plays a substantially different role depending upon the polarimetric channel. In [35] the scattering of a cloud of identical spherical particles was used to demonstrate the role of multiple scattering. The target was modeled by a diagonal Mueller matrix which in turn corresponds to a diagonal coherency matrix. In [36] the effect of multiple scattering in forest canopies at L- and C-band was studied. It was shown that the influence of multiple scattering was specially noticeable in the cross-polar channel at C-band. Also in [33] the multiple scattering component is regarded as a matrix structure whose diagonal terms are dominant. These ideas suggest that the multiple scattering component in (3) can be further simplified to a diagonal coherency matrix in the form of (4):

$$\mathbf{T_{ms}} = f_{ms} \begin{bmatrix} t_{11}^{ms} & 0 & 0 \\ 0 & t_{22}^{ms} & 0 \\ 0 & 0 & t_{33}^{ms} \end{bmatrix} \tag{4}$$

One possibility to characterize Eq. (4) for inversion purposes consists of adopting the original random distribution of dipoles proposed by Freeman and Durden [17] since it still remains as a simple and physically-based method to characterize the source of the increase of entropy within a distributed target (see discussion in Section 2). With such an assumption, the final model for parameter retrieval is given by Eq. (5):

$$\begin{aligned} \mathbf{T} \;=\; & f_s \begin{bmatrix} 1 & \beta^* \cdot \mathrm{sinc}2\psi & 0 \\ \beta \cdot \mathrm{sinc}2\psi & \frac{1}{2}|\beta|^2 \cdot (1 + \mathrm{sinc}4\psi) & 0 \\ 0 & 0 & \frac{1}{2}|\beta|^2 \cdot (1 - \mathrm{sinc}4\psi) \end{bmatrix} \\ & + f_{ms} \begin{bmatrix} \frac{1}{2} & 0 & 0 \\ 0 & \frac{1}{4} & 0 \\ 0 & 0 & \frac{1}{4} \end{bmatrix} \end{aligned} \tag{5}$$

3.1. Surface Component

Three parameters define the surface component model, namely the backscattering coefficient f_s which is common to all matrix elements, the β value, and the roughness angle ψ which represents the angular width of the distribution of angles of facets integrating the soil surface. On the one hand, β, which is a complex value, is defined in the Bragg

scattering model as [37]:

$$\beta = \frac{B_h - B_v}{B_h + B_v}, \quad |\beta| < 1 \tag{6}$$

where B_h and B_v are the Bragg scattering coefficients expressed as functions of the relative dielectric constant of the surface ε_s and the incidence angle θ. Their expressions are shown in Eq. (7):

$$\begin{aligned} B_h &= \frac{\cos\theta - \sqrt{\varepsilon_s - \sin^2\theta}}{\cos\theta + \sqrt{\varepsilon_s - \sin^2\theta}} \\ B_v &= \frac{(\varepsilon_s - 1)\left(\sin^2\theta - \varepsilon_s(1 + \sin^2\theta)\right)}{\left(\varepsilon_s \cos\theta + \sqrt{\varepsilon_s - \sin^2\theta}\right)^2} \end{aligned} \tag{7}$$

where the imaginary part of ε_s is negligigle with respect to the real part according to the electromagnetic properties of soil as a function of the wavelength [37]. Besides, the condition $|B_v| > |B_h|$ is fulfilled, which means that the real part of β is expected to be a negative value.

On the other hand, the roughness angle ψ is a key element in the X-Bragg model since it parametrizes depolarization and cross-polarization effects induced by soil roughness [5]. Actually, there are different methods [38–40] for estimating ψ which could lead to different solutions of such a parameter.

Taking into account the two considerations made before we observe that, under the X-Bragg hypothesis, the t_{12} element of the coherency matrix modeling the surface component (see Eq. (5)) must be a negative value for angular distributions between $-\pi/2$ and $\pi/2$. Nevertheless, we have observed in experimental data at C-band that the real part of the t_{12} element, i.e., $\Re(t_{12})$, can adopt both positive and negative values in high amounts. Therefore, this means that the X-Bragg model is only partially fulfilled at C-band. We have checked this behavior by analyzing both the electromagnetic response of a rough surface under controlled conditions in the EMSL facilities and the radar data acquired by RADARSAT-2 sensor. Fig. 1 shows $\Re(t_{12})$ as a function of frequency and its histogram at 5.4 GHz. The expected negative values, according to the Bragg model, appear at low frequencies and up to S-band, but from the transition between S- and C-band $\Re(t_{12})$ oscillates between negative and positive quantities. On the other hand, the histogram of $\Re(t_{12})$ at C-band shows a Gaussian-like distribution with mean around zero. Likewise, the histogram for $\Re(t_{12})$ of one of the vine parcels in our study is plotted in Fig. 2 with the corresponding photograph for reference purposes on the status of the field. As seen, there is an agreement between laboratory and real SAR data and, consequently, this shows a partial disagreement between

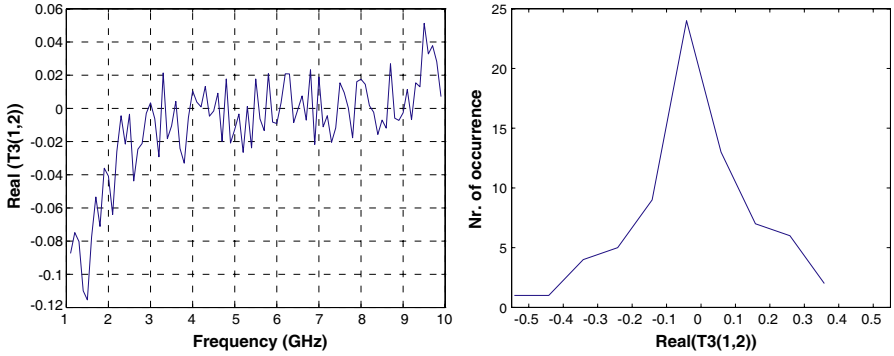

Figure 1. Statistics of $\Re(t_{12})$ for a rough surface: (a) variation as a function of frequency and (b) histogram at C-band for 72 measurements taken from different azimuth angles. Radar data acquired at the EMSL.

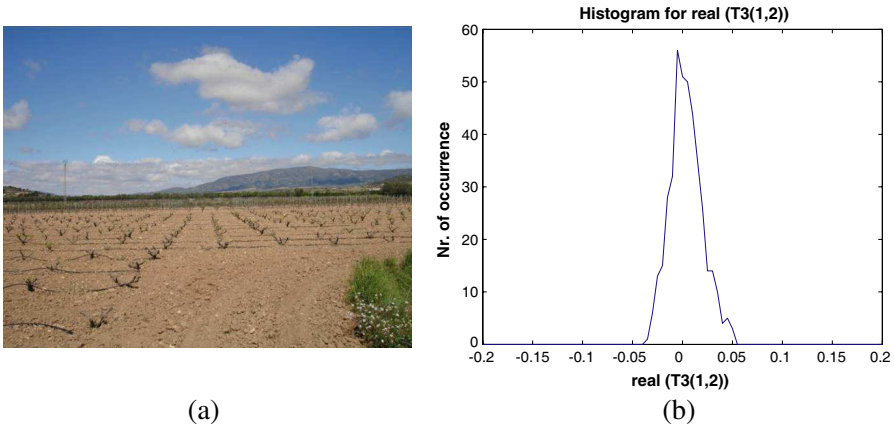

Figure 2. One of the vine parcels under study: (a) photograph and (b) histogram of $\Re(t_{12})$ for RADARSAT-2 data.

the X-Bragg model and the data set acquired at C-band which hinders the application of current approaches [11, 12] which were successfully applied to L-band data.

In order to overcome this issue, we propose to model the surface component as a hybrid X-Bragg/Fresnel model so as to give an interpretation to both the negative and the positive values for $\Re(t_{12})$.

Despite the Fresnel equations predict a null backscattering for a perfectly smooth surface, this model can be modified for accounting for

soil roughness and, hence, leading to a non-zero backscattered power. This is possible by modeling the surface by means of a collection of facets with finite size [18]. Hence, in the BSA convention the model expresses the Fresnel equations as given in Eq. (8) [18]:

$$\begin{aligned} R_h &= f(\lambda,\theta,L)\cdot\frac{\sqrt{\varepsilon_s-\sin^2\theta}-\cos\theta}{\cos\theta+\sqrt{\varepsilon_s-\sin^2\theta}} = -f(\lambda,\theta,L)\cdot B_h \\ R_v &= f(\lambda,\theta,L)\cdot\frac{\varepsilon_s\cos\theta-\sqrt{\varepsilon_s-\sin^2\theta}}{\varepsilon_s\cos\theta+\sqrt{\varepsilon_s-\sin^2\theta}} \end{aligned} \tag{8}$$

where the term $f(\lambda,\ \theta,\ L)$ depends on the wavelength λ, the incidence angle θ and the dimension of the square facet L assumed for this model. This term is given by expression (9) as:

$$f(\lambda,\theta,L) = \frac{2\sqrt{\pi}L}{\lambda}\cdot\cos\theta\cdot\mathrm{sinc}(kL\sin\theta) \tag{9}$$

According to Eqs. (8)–(9) and following the same procedure to define the surface component for the coherency matrix, a different β parameter, depending again on the soil relative permittivity and the incidence angle, is obtained. It will be denoted as β' hereafter to avoid confusion with the original β. Contrarily to β, the dynamic range of β' contains only positive values. As we will show later, this will improve the interpretation of the data and increase the performance of the inversion algorithm.

3.2. Volume Component

According to our discussion in Section 2, the second contribution of the two-component model is the random volume assumed by Freeman and Durden [17], where the only unknown is the backscattering coefficient f_{ms} (see Eq. (5)). In a recent work by Cui et al. [31] it has been shown that the volume scattering power can be uniquely determined as the minimum generalized eigenvalue of the eigenproblem defined by Eq. (2). This is the approach we adopt in this work for defining the volume component.

3.3. Further Evidences Supporting a Two-component PolSAR Model

The adoption of model given in Eq. (5) and discussed above is also supported by the analysis performed in [15] where the following behavior on the polarimetric response was found:

(i) Entropy values were confined in the 0.5–0.8 range along the whole phenological cycle.

(ii) There is one dominant eigenvalue, which associated alpha angle was always lower than 20°.

(iii) The copolar phase difference (CPD) remained low, always within ±20°.

Figures 3 and 4 show the histograms of dominant alpha and copolar phase difference for two of the parcels under study for both early and advanced phenological stages (April 19th and July 24th, respectively). The former corresponds to a bare surface with short vine stocks (see Fig. 2), and for the latter the vine morphology is fully developed in terms of LAI and plant height and the grape bunches are

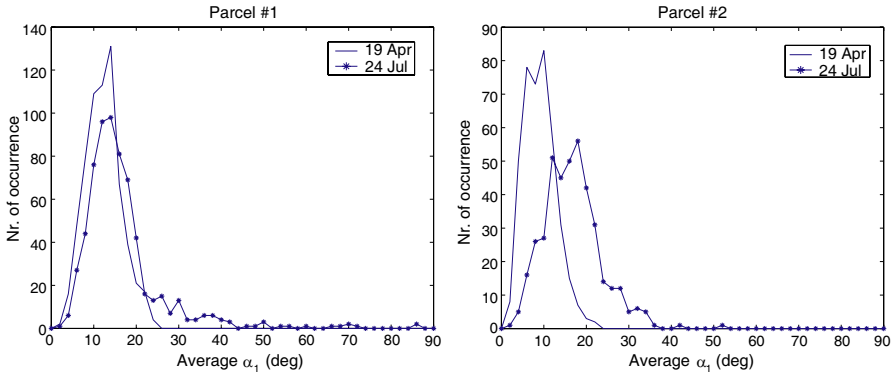

Figure 3. Histograms of α_1 for early and advanced phenological stages.

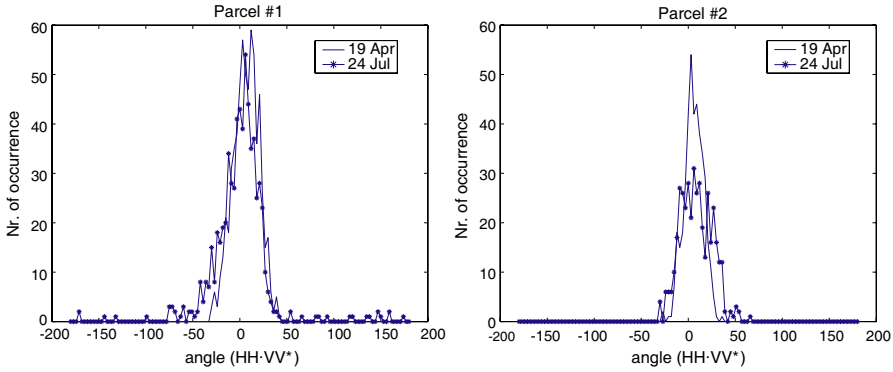

Figure 4. Histograms of $\arg(HH \cdot VV^*)$, i.e., copolar phase difference, for early and advanced phenological stages.

compact clusters. In case of α_1 the standard deviation is below 10° and in case of the CPD the highest value is 20°. These results indicate that the surface scattering coming from the ground is the dominant contribution in the whole area of both parcels.

In order to give further evidences for the interpretation above, we have also computed the conformity coefficient proposed in [41]. This coefficient is defined as in Eq. (10), where C is the covariance matrix, and $\mathrm{tr}(C)$ is the trace of C. The reflection symmetry hypothesis is assumed and it has been shown its capability for discriminating among direct surface, double-bounce and volume scattering mechanisms. The conformity value tends to unity for bare soil (copolar channels are correlated and their relative phase is zero). On the other hand, it will tend to -1 for double-bounce mechanisms (copolar channels are correlated and their relative phase is 180°). In case of volume scattering, the conformity coefficient takes an intermediate value since the HV channel is relatively large and there is a weak correlation between copolar channels. Authors in [41] found that the conformity values for volume scattering were in the range $[-0.2, 0.35]$. In Fig. 5 the histograms of the conformity coefficient for April 19 and July 24 for one of the parcels under analysis are displayed (these are similar for the other parcel). It is seen that the interpretation of surface and volume scattering mechanisms is also consistent with this coefficient.

$$\mu = \frac{2 \cdot \Re(C_{13}) - C_{22}}{\mathrm{tr}(C)} \tag{10}$$

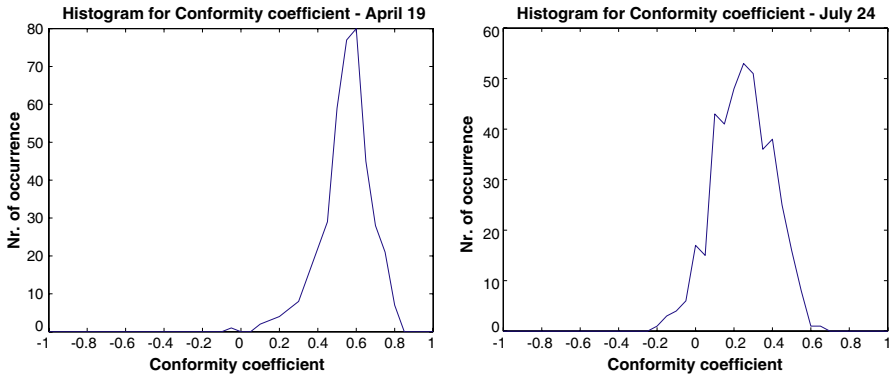

Figure 5. Histograms of conformity coefficient for early (April 19) and advanced phenological stages (July 24).

3.4. Alternative Approaches

Other alternative approaches found in the literature were previously tested before considering the proposed model as the best option for the particular scenario we study in this paper. In particular we tested the approach proposed by Jagdhuber et al. [12] for a single incidence angle and considering a random volume for modeling the vines canopy. Also, a more flexible model propose by Antropov et al. [26] was also implemented since it makes use of the copolarized ratio and the copolar cross-correlation as fitting factors. However, as authors state in [26], we did not find important differences in terms of scattering mechanisms with respect to the Freeman-Durden approach. In any case, this preliminary work gave us an additional evidence that the two-component model was physically possible for characterizing vineyards since a dominant direct surface component was consistently estimated, whereas the double-bounce contribution was negligible.

Additionally, a hybrid procedure consisting on an eigendecomposition of the coherency matrix for first extracting the dominant polarized component [31] was also tested. Once this single component was estimated, the remainder was associated with the disturbing effects of higher roughness soil areas and vines canopy. In these tests we observed that the t_{11} element of the coherency matrix was systematically assigned to the f_s backscattering coefficient of the dominant surface contribution and, hence, the secondary volume component was made up by a diagonal matrix expressed as (0, 1, 1). Therefore, these results did not yield any positive conclusion since the solutions were not consistent with the physical model proposed.

4. SOIL MOISTURE INVERSION ALGORITHM

Following our reasoning we propose an inversion algorithm for soil moisture suitable for environments where the direct surface response is the strongest contribution to the radar echoes and where the vegetation layer together with variations of terrain roughness act as a source of depolarization which is accounted for as disturbing effects on the dominant polarized signature from soil surface.

Figure 6 shows the flowchart of the inversion algorithm. The starting point is the coherency matrix $\mathbf{T}$ estimated by applying a multi-look filter (e.g., 7×7 refined Lee filter in this particular example). Then, the deorientation procedure proposed by An et al. [22] is applied. This method rotates the coherency matrix a certain angle about the line of sight to minimize the cross-polar channel and allows to redistribute the power from it to the copolar ones. By doing so, it avoids the cases where $t_{33} > t_{22}$ which would affect negatively the

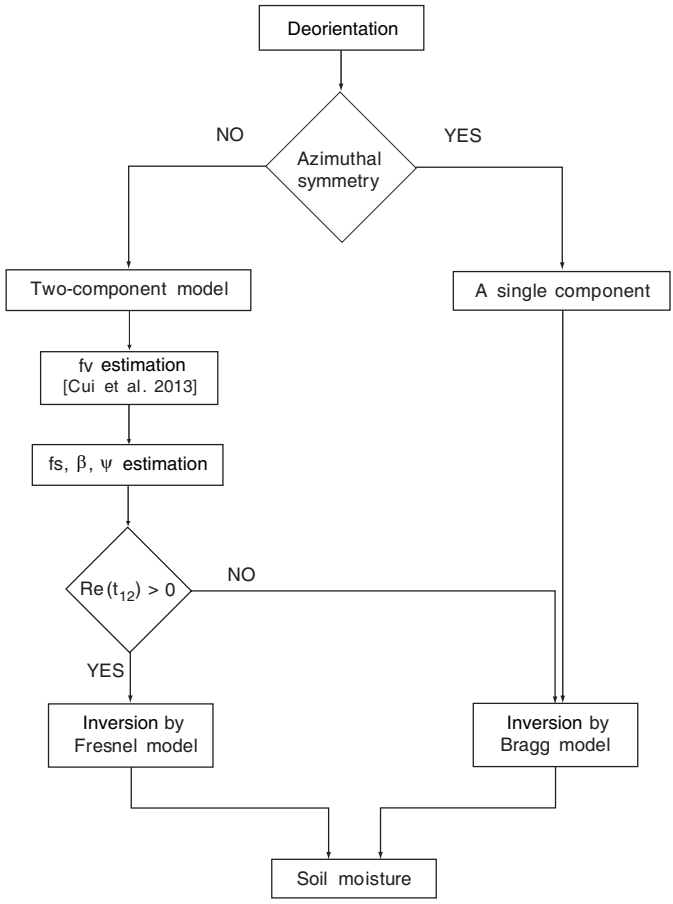

Figure 6. Flowchart of the proposed inversion algorithm for vineyards.

inversion performance (see Section 5). Additionally, it has been proven that the orientation compensation reduces the correlation between copolar and cross-polar channels [42] and, hence, this leads to a relaxation of the reflection symmetry assumption [32].

After deorientation, the structure of the new matrix $\mathbf{T}'$ is analyzed to check whether full azimuthal symmetry is fulfilled or not. We have used an empirical test consisting in calculating the ratio of the minimum between t_{22} and t_{33} over $|t_{12}|$. From several tests we have performed over the available data sets we have observed that the inversion performance increases and saturates when this ratio is about 10 dB. Hence, this threshold is set to that value. This is a necessary

step since we have observed in our tests that a number of pixels exhibits this behavior and, hence, the surface component must be modified from expression in Eq. (5) to the expression in Eq. (11):

$$\mathbf{T_{surf}} = f_s \begin{bmatrix} 1 & 0 & 0 \\ 0 & \frac{1}{2}|\beta|^2 & 0 \\ 0 & 0 & \frac{1}{2}|\beta|^2 \end{bmatrix} \tag{11}$$

Once the full azimuthal symmetry condition has been checked, the next step consists in estimating the volume component by solving the eigenproblem defined by Eq. (2) [31]. Then, the roughness angle ψ and the surface parameters f_s and β are calculated. Note that when the pixel satisfies the azimuthal symmetry case, the surface is modeled just by f_s and $|\beta|$ but not by ψ. In such a case, the soil moisture value is inverted from $|\beta|$ by means of the Bragg model.

Subtraction of the term $f_v/4$ to both t_{22} and t_{33} elements of the deoriented matrix $\mathbf{T}'$ leads to the estimation of roughness angle ψ since the new t'_{22} and t'_{33} elements are:

$$\begin{aligned} t'_{22} &= \frac{1}{2}|\beta|^2 \cdot (1 + \mathrm{sinc}(4\psi)) \\ t'_{33} &= \frac{1}{2}|\beta|^2 \cdot (1 - \mathrm{sinc}(4\psi)) \end{aligned} \tag{12}$$

The ratio of both equations in expression (12) gives the relationship in (13) [39] which allows to find ψ.

$$\frac{t'_{22}}{t'_{33}} = \frac{1 + \mathrm{sinc}(4\psi)}{1 - \mathrm{sinc}(4\psi)} \longrightarrow \mathrm{sinc}(4\psi) = \frac{\frac{t'_{22}}{t'_{33}} - 1}{\frac{t'_{22}}{t'_{33}} + 1} \tag{13}$$

After estimation of the volume component and the roughness angle, the f_s and β parameters are computed as in (14):

$$\begin{aligned} f_s &= t'_{11} = t_{11} - \frac{f_v}{2} \\ \beta &= \frac{t^{*\prime}_{12}}{f_s \cdot \mathrm{sinc}(2\psi)} \end{aligned} \tag{14}$$

The following step checks the real part of the t'_{12} element. Once the sign of $\Re(t'_{12})$ is known, the retrieval of the permittivity constant either from the Bragg or the Fresnel model is performed accordingly. Finally, the soil moisture value is obtained from the permittivity constant by inverting the expression by Topp et al. [43] given in expression (15) as:

$$m_v(\%) = -5.3 + 2.92 \cdot \varepsilon_s - 0.055 \cdot \varepsilon_s^2 + 0.0004 \cdot \varepsilon_s^3 \tag{15}$$

5. ASSESSMENT OF THE POLARIMETRIC MODEL

The assessment of both the polarimetric model and the inversion algorithm has been carried out by using RADARSAT-2 images acquired in 2010 over vineyards located in Monòver (Alicante, Spain). A total of 17 SAR images in fine quad-pol mode were acquired covering the whole phenological cycle, with 34° and 39° incidence angles. The monitored area contained six vine parcels, three of them drip irrigated and three non-irrigated. All the vineyards were sprawling canopies with no trellis system or supporting structures. The ground-truth campaign consisted in measurements of plant height, LAI, phenology stage, and the soil moisture, among other physiological parameters. It must be noted that only one single measurement of soil moisture was performed within every parcel. The reader is referenced to [15] for more details on the SAR data and ground-truth campaigns.

In this work we have limited our study to two different parcels among those analyzed in [15]. Their main features are listed in Table 1. The soil moisture values exhibit two different and nearly constant values for the first and second halves of the cycle, i.e., from April to June and from June to September, respectively. Therefore, we have selected two images corresponding to both periods as representatives of both stages. These images were acquired on April 19 and July 24 at a 34° incidence (FQ15 beam). Soil moisture values are summarized in Table 2.

5.1. Results

Figure 7 displays the retrieved soil moisture maps for parcels 1 (top row) and 2 (bottom row) on April 19, June 06 and July 24 (left to

Table 1. Characteristics of the parcels in the study area.

Parcel	Area (ha)	Ground slope (%)	Vine spacing (m)	Row spacing (m)	Irrigation system	Lat/Lon coordinates
1	2.83	3.5	2.4	2.6	unirrigated	38.457°/−0.917°
2	1.16	1.9	1.9	2.3	drip	38.432°/−0.926°

Table 2. Soil moisture of the parcels in the study area.

	Parcel 1	Parcel 2
April–June	20–25%	10%
June–Sept.	5%	5%

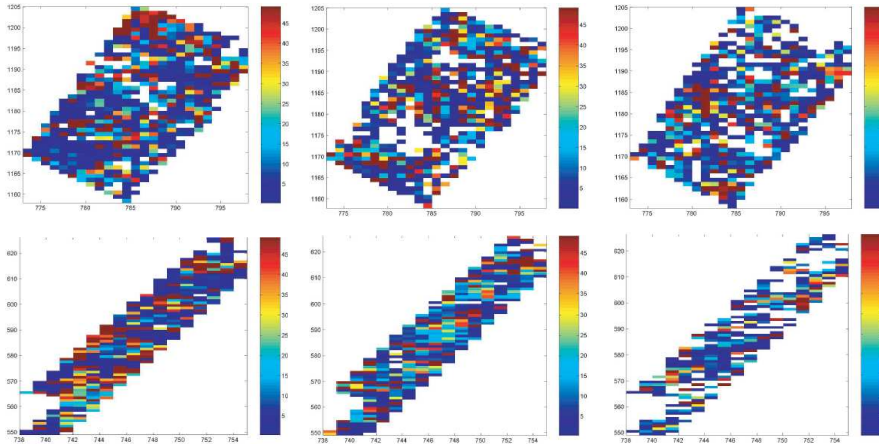

Figure 7. Soil moisture maps (%) for both parcels and dates April 19, June 06 and July 24.

right). According to these results, most of pixels are associated with low soil moisture values, not higher than 10–12%. Several spots around 15–20% are also visible (light blue color) as well as smaller areas with values higher than 35% (orange and red colors). White gaps represent pixels where non-feasible values were retrieved. In general, the inversion model is able to catch a high spatial variability of soil moisture at parcel level. This can be also seen in the histograms for the retrieved values of relative permittivity and soil moisture for both parcels, shown in Fig. 8. The procedure yields a high amount of soil moisture values below 15–20%, i.e., a permittivity about 8–10. Also, note that the histograms are dominated by extreme values of permittivity corresponding to 2 and 40. This is a consequence of the reduced dynamic range of the β and β' parameters and further analysis is required in order to understand the impact of such an issue. Actually, the lack of detailed ground-truth samples (only one single point per parcel is available) prevents any complete statistical assessment on the algorithm performance in terms of final soil moisture estimates. Nevertheless, we can provide an assessment of the consistency of the model in terms of the number of pixels that match the polarimetric characterization proposed in Section 3, i.e., the inversion rate, which gives an insight on the validity of the retrieval procedure.

Tables 3 and 4 show the inversion rates for the whole time series (seven dates starting from April 19th being the last one on September 10th) for both parcels. The retrieval procedure has been applied with and without including the data compensation by means of

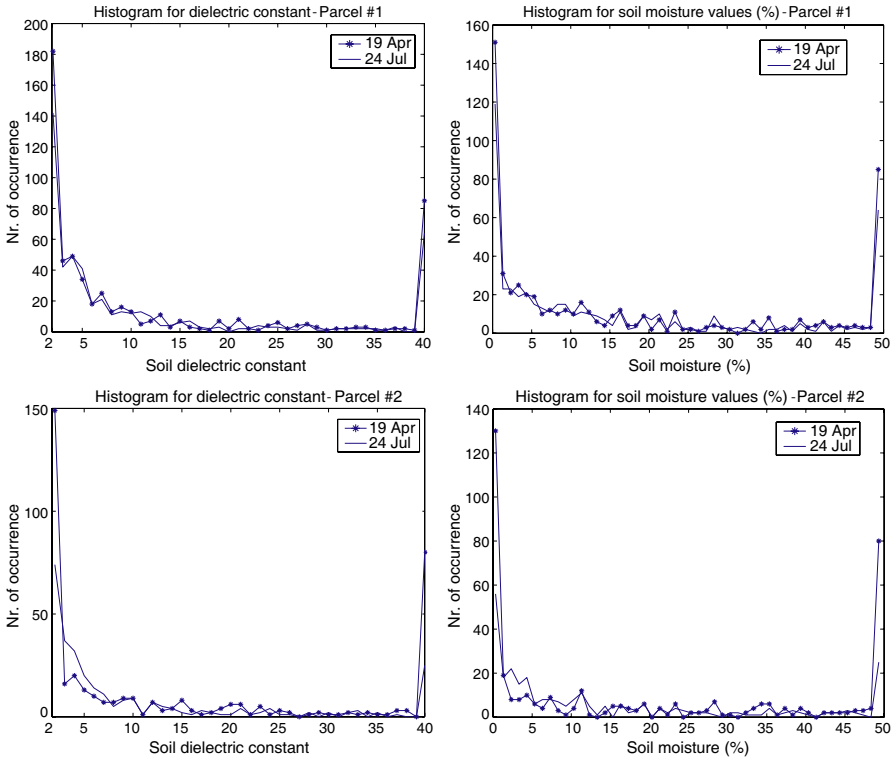

Figure 8. Histograms of permittivity and soil moisture (%) for both parcels and April 19 and July 24.

Table 3. Inversion rates for parcel 1.

	April 19	May 13	June 6	June 30	July 24	Aug. 17	Sep. 10
With deorient.	90.1%	91.48%	81.58%	92.41%	77.86%	83.9%	85.75%
No deorient.	83.75%	83.12%	73.06%	85.76%	65.63%	73.53%	74.46%

Table 4. Inversion rates for parcel 2.

	April 19	May 13	June 6	June 30	July 24	Aug. 17	Sep. 10
With deorient.	97.05%	97.29%	95.57%	76.65%	70.51%	70.02%	79.12%
No deorient.	93.61%	97.05%	94.6%	73.71%	64.86%	70.02%	72.72%

deorientation. As seen in both tables the application of deorientation improves the inversion rate up to 12% in parcel 1 and up to about 6% in case of parcel 2.

Considering the results for the compensated data, the overall conclusions on the validity of the model are different depending upon the parcel under analysis. In case of parcel 1 the inversion rate experiences some oscillations but does not take values below 81% for all dates but for the one on July 24th where a 77.86% is achieved. However, parcel 2 exhibits a clearly different behavior for two periods of the phenological cycle. For the first period, which extends from April 19th to June 6th, it exhibits inversion rates not below 95%. It must be noted that this period covers three different scenarios, namely: 1) the image on April 19th corresponds to the scenario depicted in Fig. 2 where a bare surface containing small vine stocks is present; 2) the image on May 13th corresponds to the phenological scale known as *fruit set* [44] and the LAI is slightly below $0.4\,\mathrm{m}^2/\mathrm{m}^2$; 3) the image on June 6 (see Fig. 9 for visual reference) is a key moment on vineyards development since there happens a jump in LAI up to $0.8\,\mathrm{m}^2/\mathrm{m}^2$ (the maximum for this parcel is $1\,\mathrm{m}^2/\mathrm{m}^2$). Therefore, according to this first stage, it can be concluded that the polarimetric model is well adapted to the changes in the vineyards scenario.

On the other hand, for the second set of images, which spreads from June 30 to September 10, the inversion rate has decreased significantly and oscillates between 70% and 79%. These differences on the inversion rates depending upon both the parcel and the phenological period suggest that there exist additional features still not

Figure 9. Picture of parcel 2 on June 6th.

well identified and that their effects vary depending upon the particular parcel.

5.2. Sources of Inconsistencies

Obviously, all models and inversion procedures present inconsistencies when applied to real SAR data. In this study we have identified several issues that may affect the retrieval performance:

(i) The limited dynamic range of β and β' parameters for Bragg and Fresnel formulations, respectively. Fig. 10 shows the theoretical values of β and β' and the experimental values retrieved on July 24 for parcel 1. As seen, there is a subset of both β and β' values falling outside the physically realizable interval (around 22% as shown in Table 3). This is an intrinsic drawback of the surface model and it is also exhibited in experiments at L-band over several types of crops [12]. Hence, electromagnetic modeling efforts towards an improved surface characterization are required [14, 45, 46].

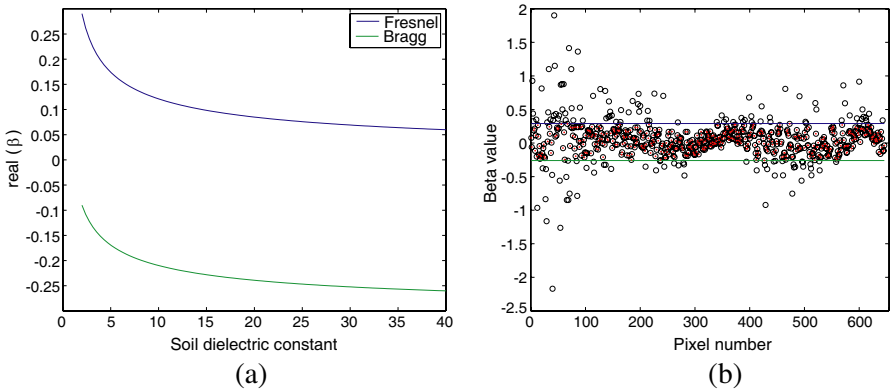

Figure 10. (a) Theoretical dynamic range of Bragg and Fresnel models for 34° incidence angle and (b) retrieved values of β and β' on July 24 for parcel 1. Blue and green horizontal lines in (b) represent the maximum and minimum value predicted by Fresnel and Bragg models, respectively. Red dots inside the circles correspond to feasible values of both β and β'.

(ii) The balance between the volume component (i.e., multiple scattering events due to both the high roughness at C-band and the volume scattering from vine plants) and the polarized

component from soil is a key factor for the suitability of the model. Actually, this is the key problem faced by polarimetric decompositions which has not been fully understood so far (see Section 2). The experimental evidences we have found (see Section 3.3) suggest that this particular scenario is a perfect candidate to be modeled by a dominant surface component and a second weak depolarizing contribution. Nevertheless, we have observed in our tests that even though the total volume power is statistically lower than that for the surface component, the consistency of the model becomes more limited as the volume-to-surface ratio gets higher, i.e., as the volume contribution is not weak when compared to the surface one. Histograms of such a ratio for all dates have been computed and plotted in Fig. 11. By inspecting the inversion rates on June 6 and June 30 for both parcels in Tables 3 and 4 and comparing them to histograms in Fig. 11 one can see a clear correlation between both indicators. The more the maximum of the histogram shifts to the left, the higher the inversion rate will be. This statement results evident when observing the differences between June 6 and June 30 for parcel 1 where the inversion rates are 81.58% and 92.41%, respectively. This improvement is reflected in the histograms for both dates (dotted and dashed lines for June 6 and June 30, respectively). From these results, we can state that the two-component model fits these data in a 80% or higher percentage whenever the volume-to-surface ratio remains around 50% or below, i.e., the volume response is 3 dB or more below the

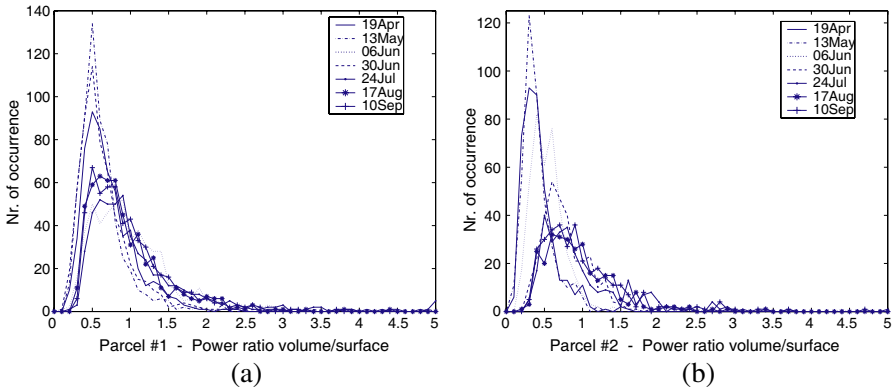

Figure 11. Histograms of volume-to-surface ratio for all dates for (a) parcel 1 and (b) parcel 2.

surface response. On the contrary, the inversion rate will decrease below 80%.

(iii) The imaginary part of β is commonly ignored. However, the inspection of experimental data reveals that this term could be significant and additional effects should be included in the model to properly account for them. In Fig. 12(a) the ratio between imaginary and real parts of element t_{12} is plotted against the frequency for the EMSL data, which shows that even at lower frequencies the term $\Im(t_{12})$ is at least of the same order as $\Re(t_{12})$. In Fig. 12(b) the histograms of such a ratio at L- and C-band suggest that this issue could affect in the same way both frequency bands.

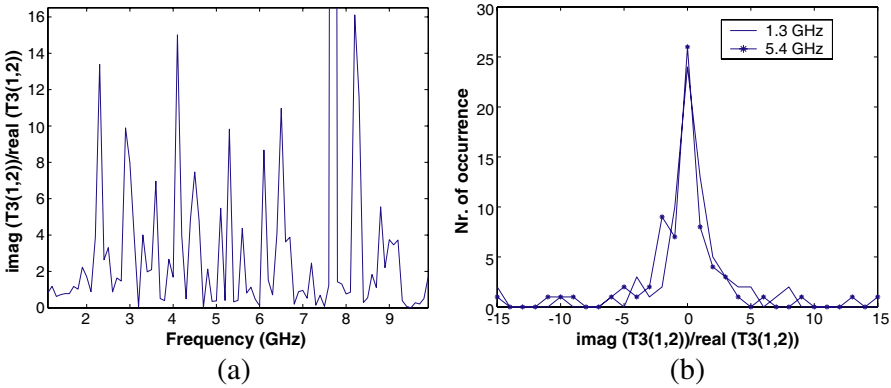

Figure 12. (a) Ratio between imaginary and real parts of element t_{12}; (b) Histograms of the ratio at L- and C-band. SAR data acquired at the EMSL.

(iv) According to our data and despite the application of the orientation angle compensation, the reflection symmetry assumption is not fully fulfilled. This point needs further research in order to better understand the impact of such approximation in the performance of the algorithm. The next step should tackle the design of an approach based on the usage of the fully polarimetric information [31].

(v) Another source of uncertainty is the lack of soil texture information since it could affect the conversion from dielectric properties of soil to the corresponding moisture values [3].

6. SUMMARY

This paper constitutes a follow-up contribution on the topic of vineyards monitoring by means of radar sensors and specifically we have focused in soil moisture estimation. In a previous work we defined this type of natural target as a two-component scenario and in the present paper the corresponding polarimetric SAR model is designed based on previous PolSAR models found in the literature. This scenario is made up of one dominant direct return from the soil and a multiple scattering component accounting for disturbing and non-modeled signal fluctuations from soil and short vegetation. We have further analyzed the polarimetric indicators that give support to such a model and we have proposed a combined X-Bragg/Fresnel approach to characterize the polarized direct response from soil. Validation of polarimetric model has been performed in terms of its consistency with respect to the available data. Also, the analysis of laboratory data gathered at the EMSL over a rough surface gives support to these statements. High inversion rates are reported for different phenological stages of vines and according to the results presented here the model gives a consistent interpretation of the data as long as the volume component power remains about or below 50% of the surface component power. Validation in terms of the accuracy of soil moisture retrieval has not been possible due to the scarcity of ground measurements and an extensive campaign is required to fully demonstrate the validity of the model. Different sources of mismatches between the model and the data have been also discussed and analyzed.

Alternative configurations also deserve attention since they could contribute to improve the performance of this approach for soil moisture retrieval over vineyards. On the one hand, it is expected that the use of an L-band polarimetric sensor will greatly improve the inversion results because of both the higher contrast between ground and vegetation and the lower impact of soil roughness [13]. On the other hand, the model-based decomposition strategies applied to PolInSAR observables could potentially lead to a better retrieval performance through the separation of coherency/covariance interferometric matrices expressed in terms of ground and canopy parameters [47–49].

ACKNOWLEDGMENT

All RADARSAT-2 images were provided by MDA and CSA in the framework of project SOAR EU 6818. RADARSAT-2 Data and Products ©MacDonald, Dettwiler and Associates Ltd. (2010) — All

The authors would like to thank the personnel of the European Microwave Signature Laboratory (EMSL) for their support in performing the indoor measurements and providing the experimental data.

This work was supported by the Spanish Ministry of Economy and Competitiveness (MINECO) and EU FEDER, under Project TEC2011-28201-C02-02.

Authors would like to thank Idoia Garmendia-Lopez and Victor J. Mangas-Martin from the University of Alicante for their work in the ground-truth campaign. Authors would also like to thank Thomas Jagdhuber from DLR for sharing his ideas and valuable suggestions.

REFERENCES

1. Oh, Y., K. Sarabandi, and F. T. Ulaby, "An empirical model and an inversion technique for radar scattering from bare soil surfaces," *IEEE Trans. on Geosci. Remote Sensing*, Vol. 30, 370–381, 1992.
2. Dubois, P. C., J. van Zyl, and T. Engman, "Measuring soil moisture with imaging radars," *IEEE Trans. on Geosci. Remote Sensing*, Vol. 33, 915–926, 1995.
3. Loew, A., R. Ludwig, and W. Mauser, "Derivation of surface soil moisture from ENVISAT ASAR wide swath and image mode data in agricultural areas," *IEEE Trans. on Geosci. Remote Sensing*, Vol. 44, No. 4, 889–899, 2006.
4. Song, K., X. Zhou, and Y. Fan, "Retrieval of soil moisture content from microwave backscattering using a modified IEM model," *Progress In Electromagnetics Research B*, Vol. 26, 383–399, 2010.
5. Hajnsek, I., E. Pottier, and S. R. Cloude, "Inversion of surface parameters from polarimetric SAR," *IEEE Trans. on Geosci. Remote Sensing*, Vol. 41, No. 4, 727–744, Apr. 2003.
6. Prasad, R., R. Kumar, and D. Singh, "A radial basis function approach to retrieve soil moisture and crop variables from X-band scatterometer observations," *Progress In Electromagnetics Research B*, Vol. 12, 201–217, 2009.
7. Singh, D., V. Srivastava, B. Pandey, and D. Bhimsaria, "Application of neural network with error correlation and time evolution for retrieval of soil moisture and other vegetation variables," *Progress In Electromagnetics Research B*, Vol. 15, 245–265, 2009.

8. Oh, Y., S.-G. Kwon, and J.-H. Hwang, "Soil moisture detection algorithm at X-band," *3rd International Asia-Pacific Conference on Synthetic Aperture Radar*, 1–4, 2011.
9. Srivastava, H. S., P. Patel, Y. Sharma, and R. R. Navalgund, "Large-area soil moisture estimation using multi-incidence-angle RADARSAT-1 SAR data," *IEEE Trans. on Geosci. Remote Sensing*, Vol. 47, No. 8, 2528–2535, 2009.
10. Gherboudj, I., R. Magagi, A. A. Berg, and B. Toth, "Soil moisture retrieval over agricultural fields from multi-polarized and multi-angular RADARSAT-2 SAR data," *Remote Sensing of Environment*, Vol. 115, No. 1, 33–43, 2011.
11. Hajnsek, I., T. Jagdhuber, H. Schön, and K. P. Papathanassiou, "Potential of estimating soil moisture under vegetation cover by means of PolSAR," *IEEE Trans. on Geosci. Remote Sensing*, Vol. 47, No. 2, 442–454, 2009.
12. Jagdhuber, T., I. Hajnsek, A. Bronstert, and K. P. Papathanassiou, "Soil moisture estimation under low vegetation cover using a multi-angular polarimetric decomposition," *IEEE Trans. on Geosci. Remote Sensing*, Vol. 51, No. 4, 2201–2214, 2012.
13. Jagdhuber, T., I. Hajnsek, and K. P. Papathanassiou, "Polarimetric decompositions for soil moisture retrieval from vegetated soils in TERENO observatories," *6th POLInSAR Workshop Frascati*, Italy, Jan. 2013.
14. Martone, M., T. Jagdhuber, I. Hajnsek, and A. Iodice, "Modified scattering decomposition for soil moisture estimation from polarimetric X-band data," *IEEE GOLD Remote Sensing Conference*, 2010.
15. Ballester-Berman, J. D., I. Garmendia-Lopez, J. M. Lopez-Sanchez, and V. J. Mangas-Martin, "Analysis of the polarimetric response of vineyards at C-band," *Canadian Journal of Remote Sensing*, Vol. 38, No. 3, 223–239, 2012.
16. Freeman, A. and S. L. Durden, "A three component scattering model to describe polarimetric SAR data," *SPIE, Radar Polarimetry*, Vol. 1748, 213–224, 1992.
17. Freeman, A. and S. L. Durden, "A three-component scattering model for polarimetric SAR data," *IEEE Trans. on Geosci. Remote Sensing*, Vol. 36, No. 3, 963–973, May 1998.
18. Cloude, S. R., *Polarisation: Applications in Remote Sensing*, Oxford University Press, 2009.
19. Yamaguchi, Y., T. Moriyama, M. Ishido, and H. Yamada, "Four-component scattering model for polarimetric SAR image

decomposition," *IEEE Trans. on Geosci. Remote Sensing*, Vol. 43, No. 8, 1699–1706, 2005.

20. Van Zyl, J. J., M. Arii, and Y. Kim, "Requirements for modelbased polarimetric decompositions," *Proceedings of EUSAR Friedrichshafen*, Germany, Jun. 2008.
21. Van Zyl, J. J., M. Arii, and Y. Kim, "Model-based decomposition of polarimetric SAR covariance matrices constrained for non-negative eigenvalues," *IEEE Trans. on Geosci. Remote Sensing*, Vol. 49, No. 9, 3452–3459, 2011.
22. An, W., Y. Cui, and J. Yang, "Three-component model-based decomposition for polarimetric SAR data," *IEEE Trans. on Geosci. Remote Sensing*, Vol. 48, No. 6, 2732–2739, 2010.
23. Huynen, J. R., "Phenomenological theory of radar targets," Ph.D. Thesis, Technical University, Delft, The Netherlands, 1970.
24. Xu, F. and Y. Q. Jin, "Deorientation theory of polarimetric scattering targets and application to terrain surface classification," *IEEE Trans. on Geosci. Remote Sensing*, Vol. 43, No. 10, 2351–2364, 2005.
25. Lee, J.-S., D. L. Schuler, and T. L. Ainsworth, "Polarimetric SAR data compensation for terrain azimuth slope variation," *IEEE Trans. on Geosci. Remote Sensing*, Vol. 38, No. 5, 2153–2163, 2000.
26. Antropov, O., Y. Rauste, and T. Häme, "Volume scattering modeling in PolSAR decompositions: Study of ALOS PALSAR data over boreal forest," *IEEE Trans. on Geosci. Remote Sensing* Vol. 49, No. 10, 3838–3848, 2011.
27. Freeman, A., "Fitting a two-component scattering model to polarimetric SAR data from forests," *IEEE Trans. on Geosci. Remote Sensing*, Vol. 45, No. 8, 2583–2592, 2007.
28. Arii, M., J. J. van Zyl, and Y. Kim, "A general characterization for polarimetric scattering from vegetation canopies," *IEEE Trans. on Geosci. Remote Sensing*, Vol. 48, No. 9, 3349–3357, 2010.
29. Arii, M., J. J. van Zyl, and Y. Kim, "Adaptive model-based decomposition of polarimetric SAR covariance matrices," *IEEE Trans. on Geosci. Remote Sensing*, Vol. 49, No. 3, 1104–1113, 2011.
30. Chen, S.-W., X.-S. Wang, Y.-Z. Li, and M. Sato, "Adaptive modelbased polarimetric decomposition using PolInSAR coherence," *IEEE Trans. on Geosci. Remote Sensing*, Vol. PP, No. 99, 1, 2013.
31. Cui, Y., Y. Yamaguchi, J. Yang, H. Kobayashi, S.-E. Park, and G. Singh, "On complete model-based decomposition of

polarimetric SAR coherence matrix data," *IEEE Trans. on Geosci. Remote Sensing*, 2013, 10.1109/TGRS.2013.2257603.

32. Lee, J.-S., T. L. Ainsworth, and Y. Wang, "Generalized polarimetric model-based decompositions using incoherent scattering models," *IEEE Trans. on Geosci. Remote Sensing*, Vol. PP, No. 99, 1–18, 2013, 10.1109/TGRS.2013.2262051.
33. Allain, S., "Caractérisation d'un Sol nu à partir de données SAR Polarimétriques: Etude Multi-fréquentielle et Multi-résolutions," Ph.D. Thesis, University of Rennes, France, 2003.
34. Lopez-Sanchez, J. M., S. R. Cloude, and J. D. Ballester-Berman, "Rice phenology monitoring by means of SAR polarimetry at X band," *IEEE Trans. on Geosci. Remote Sensing*, Vol. 50, No. 7, 2695–2709, 2012.
35. Cloude, S. R. and E. Pottier, "An entropy based classification scheme for land applications of polarimetric SAR," *IEEE Trans. on Geosci. Remote Sensing*, Vol. 35, No. 1, 68–78, Jan. 1997.
36. Wang, Y., J. F. Paris, and F. W. Davis, "Inclusion of a simple multiple scattering model into a microwave canopy backscatter model," *Remote Sensing of Environment*, Vol. 63, No. 2, 101–111, 1998.
37. Ulaby, F. T., R. K. Moore, and A. K. Fung, *Microwave Remote Sensing: From Theory to Applications*, Vol. III, Artech House, 1986.
38. Mattia, F., T. Le Toan, J.-C. Souyris, G. de Carolis, N. Floury, F. Posa, and G. Pasquariello, "The effect of surface roughness on multifrequency polarimetric SAR data," *IEEE Trans. on Geosci. Remote Sensing*, Vol. 35, 954–966, 1997.
39. Cloude, S. R. and K. P. Papathanassiou, "Surface roughness and polarimetric entropy," *Proceedings of the IEEE International Geoscience and Remote Sensing Symposium (IGARSS)*, Vol. 5, 2443–2445, Hamburg, Germany, Jun. 1999.
40. Schuler, D. L., J.-S. Lee, D. Kasilingam, and G. Nesti, "Surface roughness and slope measurements using polarimetric SAR data," *IEEE Trans. on Geosci. Remote Sensing*, Vol. 40, 687–698, 2002.
41. Truong-Loi, M.-L., P. Dubois-Fernandez, A. Freeman, and E. Pottier, "The conformity coefficient or how to explore the scattering behaviour from compact polarimetry mode," *2009 IEEE Radar Conference*, 1–6, 2009.
42. Lee, J. S. and T. L. Ainsworth, "The effect of orientation angle compensation on coherency matrix and polarimetric target decompositions," *IEEE Trans. on Geosci. Remote Sensing*,

Vol. 49, No. 1, 53–64, 2011.

43. Topp, G. C., J. L. Davis, and A. P. Annan, "Electromagnetic determination of soil water content: Measurements in coaxial transmission lines," *Water Resources Research*, Vol. 16, 574–582, 1980.
44. Baggiolini, M., "Les stades repères dans le développement annuel de la vigne et leur utilisation pratique," *Revue Romande d'Agriculture et d'Arboriculture*, Vol. 8, 4–6, 1952.
45. Liang, D., P. Xu, L. Tsang, Z. Gui, and K.-S. Chen, "Electromagnetic scattering by rough surfaces with large heights and slopes with applications to microwave remote sensing of rough surface over layered media," *Progress In Electromagnetics Research*, Vol. 95, 199–218, 2009.
46. Treuhaft, R. N., S. T. Lowe, and E. Cardellach, "Formulating a vector wave expression for polarimetric GNSS surface scattering," *Progress In Electromagnetics Research B*, Vol. 33, 257–276, 2011.
47. Neumann, M., L. Ferro-Famil, and A. Reigber, "Improvement of vegetation parameter retrieval from polarimetric SAR interferometry using a simple polarimetric scattering model," *4th POLinSAR Workshop*, Frascati, Italy, Jan. 2009.
48. Ballester-Berman, J. D. and J. M. Lopez-Sanchez, "Applying the Freeman-Durden decomposition concept to polarimetric SAR interferometry," *IEEE Trans. on Geosci. Remote Sensing*, Vol. 48, No. 1, 466–479, 2010.
49. Xing, S., D. Dai, Y. Li, and X. Wang, "Polarimetric SAR tomography using $l_{2,1}$ mixed norm sparse reconstruction method," *Progress In Electromagnetics Research*, Vol. 130, 105–130, 2012.